



The Open Electrical & Electronic Engineering Journal

Content list available at: www.benthamopen.com/TOEEJ/

DOI: 10.2174/1874129001812010098, 2018, 12, 98-109



RESEARCH ARTICLE

Battery Losses In a MMC for BEVS Application

Adolfo Dannier*, Gianluca Brando, Ivan Spina and Diego Iannuzzi

Department of Electrical Engineering and Information Technologies – University of Naples Federico II, Naples, Italy

Received: June 26, 2018

Revised: September 15, 2018

Accepted: September 27, 2018

Abstract:

Objective:

This paper analyses the Modular Multilevel Converter (MMC) topology, where each individual Sub Module (SM), in half bridge configuration, is directly fed by an elementary electrochemical cell.

Methods:

The aim is to investigate how the reference voltages influence the cells currents waveforms, determining how the active powers and the losses are distributed among the cells. Considering a 2-level Voltage Source Inverter (VSI) topology working in the same conditions, the ratio between the MMC total cells losses and VSI total cells losses is calculated. After showing the system architecture and mathematical model, the cells current waveform investigation is presented and detailed both for triangular and sinusoidal voltage reference waveform.

Results:

Finally, the results are critically discussed with particular focus on the comparison between the MMC and the VSI topologies.

Keywords: CMMC topology, Battery losses, Electrical vehicles, Battery cells, BMS, DC-linked voltage.

1. INTRODUCTION

Over the last decades, several legislative regulations have been introduced with the aim to encourage and stimulate a flawless transition from traditional Internal Combustion (IC) based vehicles to Battery Electric Vehicles (BEVs) [1]. Indeed, full electric based traction drives have overall efficiency of 80% while offering zero emission of Greenhouse Gases (GHG) and other air pollutants, which, instead, are the main drawbacks of conventional vehicles. However, the public uptake of electric vehicles is strongly hampered by the reduced energy density and limited lifetime of the batteries, the low diffusion of the charging stations in both urban and extra-urban area and, last but not least, the long recharge times. In particular, the lifetime of the batteries are strictly dependent on the use of the batteries and the system architecture. Generally, since the battery is directly connected to the main DC-bus, the number of series-connections is imposed by the desired DC-link voltage, while the number of parallel-connections is subjected to the required total energy of the storage system [2]. Even though the battery cells are ideally charged or discharged by the same current, the correspondent terminal voltage and State-of-Charge (SOC) will be different because of the electrochemical characteristics differences, which would lead to an unbalanced power contribution [3] and to premature failure of the battery over extended cycling due to individual cells overcharging/undercharging. Therefore, passive or active Battery Management Systems (BMSs) are added to the battery [4] in order to dramatically increase the cells lifetime. The BMS has the main purpose of dynamically minimizing the cells imbalance during normal operations in order to preserve the battery lifetime [5]. In this approach, the traction power unit is equipped with an DC/AC converter that connects the

* Address correspondence to this author at the Department of Electrical Engineering and Information Technologies – University of Naples Federico II, Claudio 21, 80125 Naples, Italy; Tel: +390817683233; E-mail: adolfo.dannier@unina.it

DC-link to the AC-motor and/or the AC-grid [6]. Several topologies have been proposed for the main DC/AC converter with the aim to obtain good performance and high conversion efficiency. Among them, multilevel converters are considered as one of the most effective solutions [7, 8]. In particular, an alternative system architecture can be built upon the Modular Multilevel Converter (MMC) by connecting each individual Sub Module (SM), in half or full bridge configuration, to an elementary battery cell [9, 10]. Generally this converter topology is used for high voltage application, where the most significant features are: high redundancy index, reduced devices ratings, strong scalability, common DC-link for multi-drive applications, low output voltages, excellent fault-tolerance capability, and enhanced motor efficiency/performance in comparison with the traditional two-level Voltage Source Inverter (VSI) [11 - 13].

In the context of Electrical Vehicles (EVs) applications, the MMC can be viewed as a Configurable Modular Multilevel Converter (CMMC) [14, 15]. Indeed, the MMC, in both traction and charger modes, once coupled with a proper balancing control strategy, integrates also the BMS functionality, thus leading to an increased power density [16]. However, the resulting conversion efficiency could suffer given the high number of required switching devices. An extensive analysis of the semiconductor related losses has shown that the MMC-based architecture has efficiency levels comparable with VSI-based ones [17].

Moreover, since each cell delivers a current waveform which is marginally dependent on the converter output mean power, the resulting substantial difference between the RMS and DC value of the cells currents increases the losses of the storage system. This aspect is investigated in this paper, which carries out an in-depth analysis by examining the dependence between the reference cells voltages, the output converter currents and the correspondent cells losses. This approach could be useful for the development of a modulation strategy that aims to minimize the battery losses regardless of the system operating condition.

2. SYSTEM ARCHITECTURE AND MODEL

The MMC system architecture is shown in Fig. (1)

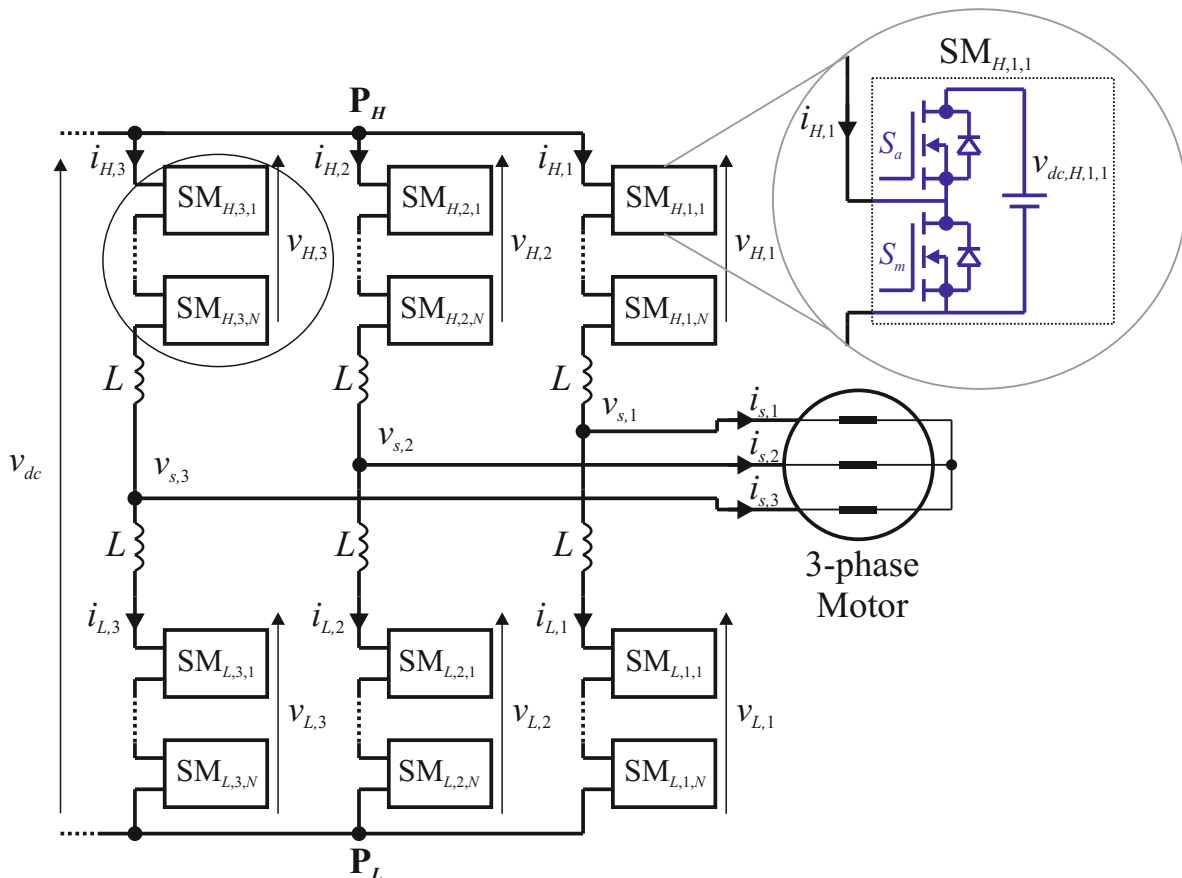


Fig. (1). Modular Multilevel Converter architecture.

The six arms of the depicted double-star cascaded three-phase converter are built upon N series connected half bridge Sub Modules (SM), each one connected to an elementary cell on the DC side. The whole structure can be seen as two cascaded converters (higher and lower) parallel-connected with respect to the load, series-connected with respect to the total DC-link. In the proposed scheme, the converter phases are connected by six identical inductors, while the total DC-link voltage v_{dk} is derived between points PH and PL. The coupling inductors are needed in order to optimize the parallel connection by properly conditioning the dynamic of the circulating currents coherently with the control time response.

The currents $i_{H,k}, i_{L,k}$ flowing in the k -th arm of the higher, lower converter can be decomposed in their circulating, load components $i_{s,k}, i_{c,k}$:

$$i_{H,k} = \frac{i_{s,k}}{2} + i_{c,k} \quad ; \quad i_{L,k} = -\frac{i_{s,k}}{2} + i_{c,k} \tag{1}$$

While the load currents $i_{s,k}$ are generally linked to the load control law and, therefore, cannot be arbitrarily chosen, the circulating currents $i_{c,k}$ are not subject to such constraints and, consequently, introduce degrees of freedom to the converter control strategy.

The total output voltages $v_{H,k}, v_{L,k}$ of the k -th arm of the higher, lower converter can be expressed as:

$$v_{H,k} = \sum_{r=1}^N S_{H,k,r} v_{dc,H,k,r} \quad ; \quad v_{L,k} = \sum_{r=1}^N S_{L,k,r} v_{dc,L,k,r} \tag{2}$$

where $S_{H,k,r}, S_{L,k,r} \in \{0,1\}$ are the switching function of the r -th module belonging to the k -phase of the higher, lower converter. The quantities $v_{dc,H,k,r}, v_{dc,L,k,r}$ are the corresponding elementary cell voltage and depends on its Status Of Charge (SOC) and its delivered current $S_{H,k,r}i_{H,k}, S_{L,k,r}i_{L,k}$.

The arm voltages $v_{H,k}, v_{L,k}$ can be decomposed in their total, differential components $v_{\sigma,k}, v_{\delta,k}$:

$$v_{H,k} = \frac{v_{\delta,k}}{2} + \frac{v_{\sigma,k}}{2} \quad ; \quad v_{L,k} = -\frac{v_{\delta,k}}{2} + \frac{v_{\sigma,k}}{2} \tag{3}$$

A better perspective with respect to the definition of the converter control strategy can be brought forth by replacing the generic phase-variables x_k with their space vector and common mode components

$\mathbf{x} = \frac{2}{3} \sum_{k=1}^3 x_k e^{j\frac{2\pi}{2}(k-1)}$, $x_0 = \frac{1}{3} \sum_{k=1}^3 x_k$. By "applying "the "Kirchhoff "voltage "laws "to the double-star converter, its mathematical model can be synthetically formulated with respect to the space vector and common mode components of $i_{s,k}, i_{c,k}, v_{\delta,k}, v_{\sigma,k}$:

$$\begin{cases} \frac{\mathbf{v}_{\delta}}{2} + \frac{L}{2} \frac{d\mathbf{i}_s}{dt} + \mathbf{v}_s = 0 \\ \mathbf{v}_{\sigma} + 2L \frac{d\mathbf{i}_c}{dt} = 0 \\ v_{\sigma,0} + 2L \frac{di_{c,0}}{dt} - v_{dc} = 0 \end{cases} \tag{4}$$

where \mathbf{v}_s is the space vector of the load phase voltages $v_{s,k}$. From (4), it is clear that, while \mathbf{v}_{δ} is calculated by the load control law, \mathbf{v}_{σ} can be used as an effective control variable by properly driving the space vector of the re-circulating current based on the MMC control strategy. Indeed, i_c can be exploited in order to equalize the SOCs of the elementary cells during the converter operation [12]. Therefore, by effectively controlling i_c and by properly distributing the output

power of each leg among the correspondent modules, the MMC is able to feed the load while keeping the cells balanced. However, an injection of a circulating current in each converter arm increases the RMS value of the currents, decreasing the total system efficiency. For this reason, in order to compare the MMC architecture to the traditional VSI one with respect to the system efficiency, i_c and v_σ are set to zero, i.e. no equalization action is performed by the control strategy. Moreover, with reference to the steady state conditions, for which $di_{c,0} / dt = 0$ for each value of the converter output modulation index, $v_{\sigma,0}$ becomes constrained to the value $\bar{v}_{\sigma,0} = \frac{1}{6} \sum_{k=1}^3 \sum_{r=1}^N (v_{dc,H,k,r} + v_{dc,L,k,r})$. Under this hypothesis, the reference arm voltages depends only on v_δ and $v_{\delta,0}$, which, as per (4), can be freely chosen. In particular, once the higher and lower converters are symmetrically modulated by imposing $v_{\delta,0} = 0$, the following relations apply:

$$v_{H,k} = \text{Re} \left\{ \frac{v_{\delta,k}}{2} e^{-j\frac{2\pi}{3}(k-1)} \right\} + \frac{\bar{v}_{\sigma,0}}{2} \quad ; \quad v_{L,k} = -\text{Re} \left\{ \frac{v_{\delta,k}}{2} e^{-j\frac{2\pi}{3}(k-1)} \right\} + \frac{\bar{v}_{\sigma,0}}{2} \quad (5)$$

From (5) it can be noted that the reference voltages of the higher and lower converters are reduced to two three-phase symmetrical systems. In this case, the analysis of the converter steady-state operation can be carried out with reference to one converter arm and extended to the whole structure.

3. WAVEFORM OF THE CELLS CURRENTS

Thanks to the high number of SMs, the load current is typically characterized by low distortion even when the cells are simply connected/disconnected based on the reference voltage value and no PWM technique is implemented. Thus, in normal steady state operation, the current waveform flowing in a specific SM cell depends on 3 factors: the actual SOC of the cell, the reference voltage waveform and the arm current waveform.

The actual SOC of the cell determines its order in the sorting algorithm and thus establishes a voltage threshold across which the cell is inserted and/or disconnected in the circuit. Consequently, the voltage reference waveform fixes the time instants when the SM related to the specific cell is switched ON and OFF. Finally, during the time intervals when the SM is kept ON, its cell experiences the arm current, while during OFF intervals the cell current is zero. In other words, the cell current is the same of the arm one except it is zero during the time intervals where the reference voltage is below the threshold; the threshold depends on the actual SOC of the cell. In Fig. (2) a generic voltage reference waveform is compared with a threshold (red line) determining the cell current waveform from a generic load current waveform.

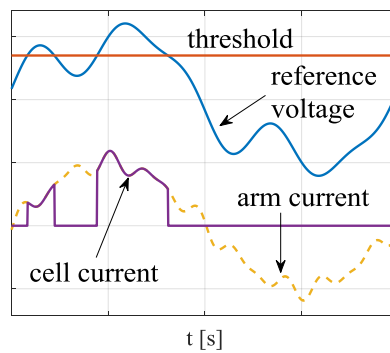


Fig. (2). Qualitative behavior of single cell reference voltage and current waveforms.

Naturally, for N cells per arm there will be N different cell current waveforms, each one instantaneously equal to the arm current in different time intervals. By consequence, each cell will supply a different active power and the sum of all cells different active powers will be equal to the load power; whereas, in traditional VSI every cell delivers the same active power. Thus, for MMC topology it is important to analyze the distribution of the active power among the cells and, in particular, to evaluate how the unbalanced power distribution influences the total cell losses.

With reference to a single arm of the converter, assuming that the converter cells are kept quite well balanced with

regard to their SOCs, they can be simply numbered according to their physical position from bottom to top (Fig. 3). In this case each cell is characterized by the same voltage V_{cell} , so that the voltage threshold value which determines the connection and disconnection of the generic k^{th} cell will be $k \cdot V_{cell}$.

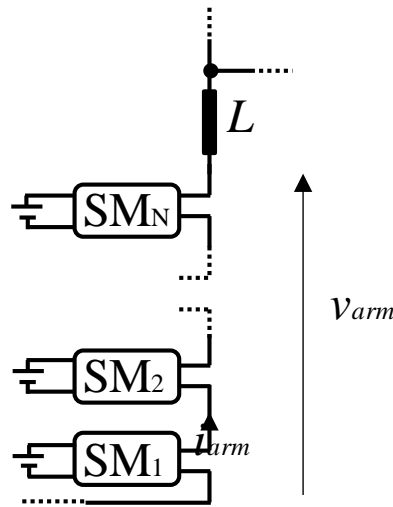


Fig. (3). Detailed representation of a generic MMC arm.

3.1. Simplified Case

For sake of simplicity, it is supposed that the MMC converter has 100 cells per arm, each characterized by a voltage value of 1 V, so that a reference voltage across 75 V would drive the ON/OFF switching of the 75th SM cell. Under this hypothesis, a voltage absolute value in [V] directly translates to a percentage one in [%].

The load current is assumed sinusoidal and synchronous with respect to the fundamental frequency of the reference voltage. Its peak value is also fixed to 200 % (200 A in the assumed case example), and placed on the peak of the voltage, *i.e.* the current is aligned with the reference voltage; the arm current peak value corresponds to 100 A (100%).

Since the magnitude and waveform of the generic arm current have been constrained, the distribution of the current among the arm cells only depends on the voltage reference waveform.

3.1.1. Triangular Reference Voltage

If the reference voltage is triangular shaped and with unitary modulation index, the current waveforms of the cells can be derived quite intuitively. Indeed the time instants t_{on} , t_{off} where the generic k^{th} cell is connected/disconnected are linearly dependent on k . For a generic k^{th} cell the situation is that of Fig. (4).

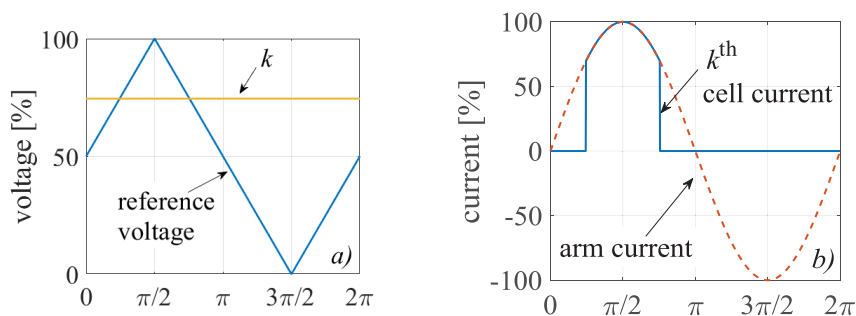


Fig. (4). k^{th} cell current waveform for triangular reference voltage.

The generic k^{th} cell current waveform depicted in Fig. (4b) can be characterized both in terms of mean value (DC value) and in terms of root mean square value (RMS value); these depending on the time instants t_{on} , t_{off} . When $k \geq 50$, t_{on} can be easily calculated by the following:

$$v_{ref} = 50 + 50 \cdot \omega t_{on} \cdot \frac{2}{\pi} = k \Rightarrow \omega t_{on} = \frac{\pi}{2} \cdot \frac{k - 50}{50} \tag{6}$$

while the time instant t_{off} corresponds to:

$$\omega t_{off} = \pi - \omega t_{on} \tag{7}$$

The active power supplied by the k^{th} cell is proportional to its DC current value; $k=50$ corresponding to the maximum power. It is worth notice that each couple of cell of the type $(100-\Delta)^{th}$ and $(1+\Delta)^{th}$ (with $\Delta=1,2,\dots,N/2-1$) have complementary current waveform Fig. (5).

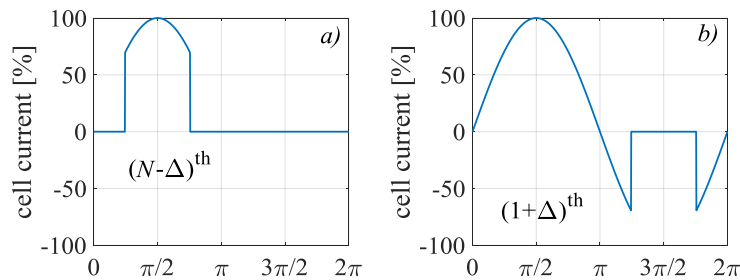


Fig. (5). Behavior of complementary cells couple current waveforms.

The DC current value of the $(100-\Delta)^{th}$ cell is equal to one of the $(1+\Delta)^{th}$ cell; the two cells deliver the same active power. Considering all the cells, the DC current values associated with first 50 cells (1^{st} - 50^{th}) correspond to the ones of the second 50 cells (51^{st} - 100^{th}).

The DC current values distribution among the 51^{st} - 100^{th} cells can be calculated from (6) and (7):

$$I_{dc,k} = \frac{1}{2\pi} \int_{\omega t_{on}}^{\omega t_{off}} 100 \sin(\omega t) \cdot d(\omega t) = \frac{100}{\pi} \left\{ \cos \left[\left(\frac{k-50}{100} \right) \pi \right] \right\} \quad 51 \leq k \leq 100 \tag{8}$$

The remaining 1^{st} - 50^{th} cells will be characterized by the same DC current values, so that the total distribution appears as in Fig. (6).

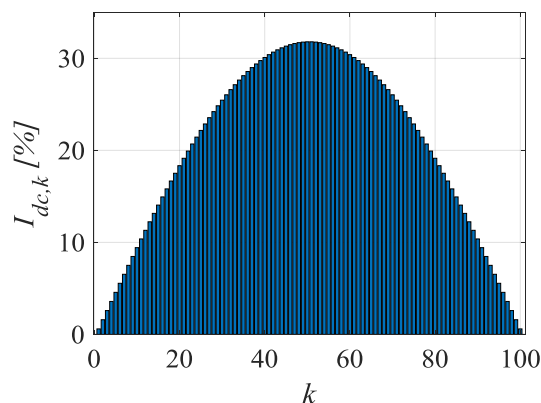


Fig. (6). Behavior of DC current values distribution with triangular reference voltage.

As expected, the distribution of $I_{dc,k}$ is sinusoidal, as a sinusoidal load current waveform has been intercepted by a linear transformation (triangular reference voltage):

$$I_{dc,k} = \frac{100}{\pi} \sin\left(\frac{\pi}{100}k\right) \quad 1 \leq k \leq 100 \tag{9}$$

The total active power supplied by the 100 cells is of course proportional to the sum of $I_{dc,k}$ and so proportional to the average value of $I_{dc,k}$. The average value of $I_{dc,k}$ can be calculated as:

$$I_{dc} = \frac{1}{100} \int_1^{100} I_{dc,k} dk \cong \frac{200}{\pi^2} = 20.2 \text{ A} \tag{10}$$

where I_{dc} is the average value of the all 100 cells DC current values.

Although $I_{dc,k}$ is different for each cell, with regard to the active power it is as each cell supply a constant current equal to I_{dc} .

With reference to Fig. (5), it is clear that, despite the cell group $(100-\Delta)^{th}$ and $(1+\Delta)^{th}$ supply the same active power, their losses are different, being different the RMS current values. In particular the RMS current values of the 1st-50th cells are higher than the ones of the 51st-100th cells. In the discussed case of triangular reference voltage, the distribution of the 100 cell RMS current values $I_{rms,k}$ is the one of Fig. (7).

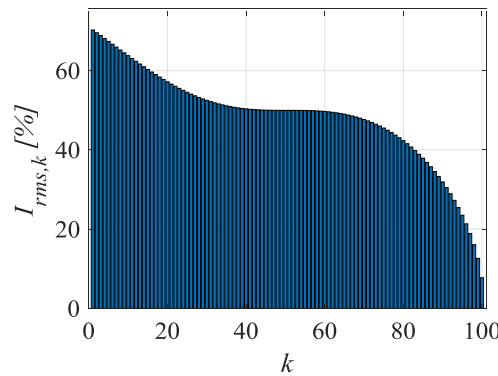


Fig. (7). Behavior of RMS current values distribution with triangular reference voltage.

The average value of all $I_{rms,k}$ can be calculated considering that each of first 50 cell (see $(1+\Delta)^{th}$ cell of Fig. 5b) experiences a current waveform equal to the arm one, except for a null interval placed between π and 2π . For each $(1+\Delta)^{th}$ cell there is a complementary $(100-\Delta)^{th}$ cell whose current waveform exactly corresponds to the missing part of $(1+\Delta)^{th}$ cell. Thus, with regard to the average value of all $I_{rms,k}$, it is as half the cells experiences the total arm current and half the cells has a zero current:

$$I_{rms} = \frac{I_{arm,rms}}{\sqrt{2}} = 50 \text{ A} \tag{11}$$

where I_{rms} is the average value of $I_{rms,k}$ among all 100 cells $I_{arm,rms}$ and is the arm current RMS value.

In a traditional VSI the series connected elementary cells will substantially supply a constant current proportional to the load power. Therefore, their losses will be associated with I_{dc}^2 . In the discussed MMC case, instead, the cells losses are associated with I_{rms}^2 . It is worth noting that the MMC cells losses are increased by a factor ξ :

$$\xi = \frac{I_{rms}^2}{I_{dc}^2} = \frac{\pi^4}{16} \cong 6 \tag{12}$$

3.1.2. Sinusoidal Reference Voltage

In normal steady state operation the 3 higher arm reference voltages are a 3-phase symmetrical sinusoidal system and each lower arm reference voltage is opposite to the correspondent higher phase one Fig. (8a). Thus, at unitary modulation index, each arm is driven in order to produce the reference voltage of Fig. (8b).

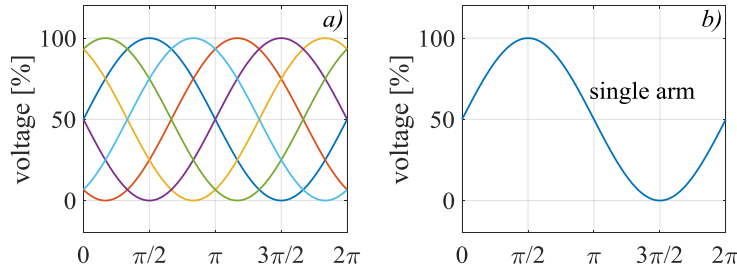


Fig. (8). Reference voltages for the higher arms (a) and for a single arm (b).

When $k > 50$, the time instant t_{on} corresponding to the connection of the cell can be easily evaluated by:

$$v_{ref} = 50 + 50 \cdot \sin(\omega t_{on}) = k \Rightarrow \omega t_{on} = \sin^{-1}\left(\frac{k-50}{50}\right) \tag{13}$$

while the time instant t_{off} is still given by (7).

The DC current values distribution among the 51th-100th cells can be calculated as:

$$I_{dc,k} = \frac{1}{2\pi} \int_{\omega t_{on}}^{\omega t_{off}} 100 \sin(\omega t) \cdot d(\omega t) = \frac{100}{\pi} \left\{ \cos \left[\sin^{-1} \left(\frac{k-50}{50} \right) \right] \right\} \quad k \in [51, 100] \tag{14}$$

The remaining 1st-50th cells will be characterized by the same DC current values of the 51th-100th ones, so that the total distribution appears as in Fig. (9).

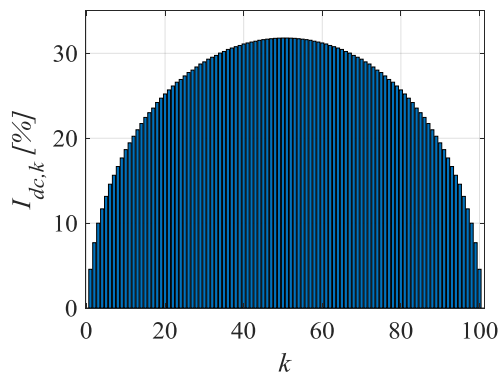


Fig. (9). Behavior of DC current values distribution with sinusoidal reference voltage.

The distribution of Fig. (9) is a semi ellipse centered at [0;50], and with vertical and horizontal axes respectively equal to 100/π and 50. Thus the average value of all 100 cells DC currents value can be calculated as:

$$I_{dc} = \frac{1}{100} \frac{1}{2} \pi \cdot \frac{100}{\pi} \cdot 50 = 25 \text{ A} \tag{15}$$

With sinusoidal reference voltage, the distribution of the RMS current values among the 100 cells appears as in Fig. (10).

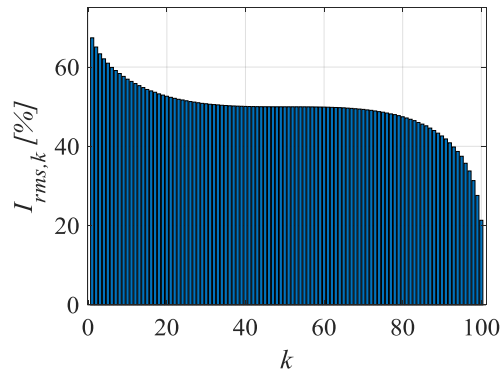


Fig. (10). Behavior of RMS current values distribution with sinusoidal reference voltage.

Although the distribution of Fig. (10) is different from the one of Fig. (7), the quantity I_{rms} doesn't change (see (11)). Consequently, the ratio ξ between I_{rms}^2 and I_{dc}^2 is:

$$\xi = \frac{I_{rms}^2}{I_{dc}^2} = 4 \tag{16}$$

3.2. General Case

A general case of N cells per arm is considered. Each cell is characterized by the voltage V_{cell} . The load current is sinusoidal with $2I_{pk}$ peak amplitude and $\cos\varphi$ power factor. The reference voltages are characterized by a modulation index set to m , and a common mode component set to $N \cdot V_{cell} / 2$.

As long as the reference voltage does not contain even harmonics, the time instants t_{on} and t_{off} corresponding to the connection and disconnection of the cell, are symmetrically placed around $\pi / 2$ or $3\pi / 2$. This still allows to find couple of cells of the type $(N-\Delta)^{th}$ and $(1+\Delta)^{th}$ having complementary current waveform and equal DC current values Fig. (11).

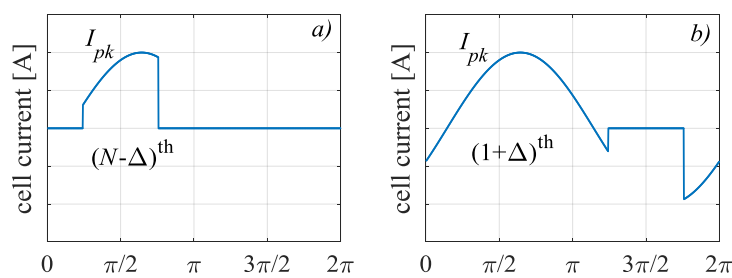


Fig. (11). Behavior of complementary cells couple current waveforms.

The DC current value of the generic k^{th} cell corresponds to:

$$I_{dc,k} = \frac{I_{pk}}{\pi} \cos(\omega t_{on}) \cos\varphi \tag{17}$$

With reference to Fig. (11), it is evident that the quantity I_{rms} still satisfies (11) and corresponds to:

$$I_{rms} = \frac{I_{arm,rms}}{\sqrt{2}} = \frac{I_{pk}}{2} \tag{18}$$

It is worth noting that, differently than in a traditional VSI, I_{rms} only depends on the load current peak value and not on the modulation index or the load power factor. If for instance m is set to zero, since the mean value of the reference voltage is $N \cdot V_{cell} / 2$, half the cells will have a current equal to zero and half the cells will experience the total arm current; I_{rms} is still given by the (18). This suggests a strong dependence of I_{rms} from the common mode component of the reference voltages.

3.2.1. Triangular Reference Voltage

With the position $z = N / 2$, for a triangular shaped reference voltage, the time instant t_{on} corresponding to the connection of the k th cell with $z < k \leq z(1 + m)$, can be easily calculated as:

$$v_{ref} = zV_{cell} + \frac{2}{\pi}mzV_{cell} \cdot \omega t_{on} = k \cdot V_{cell} \Rightarrow \omega t_{on} = \frac{\pi}{2} \cdot \frac{k - z}{mz} \tag{19}$$

Considering that each couple of cells of the type $(N-\Delta)^{th}$ and $(1+\Delta)^{th}$ have complementary current waveform, and that the k^{th} cells with $z(1 - m) < k \leq z(1 + m)$ are the only ones with a non-zero DC current value, from (17) and (19) it is easy to verify that:

$$I_{dc,k} = \frac{I_{pk}}{\pi} \cos \left[\frac{\pi}{2} \left(\frac{k - z}{mz} \right) \right] \cos \varphi \quad z(1-m) < k \leq z(1+m) \tag{20}$$

The quantity I_{dc} can then be calculated as:

$$I_{dc} = \frac{1}{N} \int_{z(1-m)+1}^{z(1+m)} I_{dc,k} dk \cong \frac{2mI_{pk} \cos \varphi}{\pi^2} \quad (mz \square 1) \tag{21}$$

As in a traditional VSI, I_{dc} depends both on the modulation index and on the load power factor. Thus, the factor ξ becomes:

$$\xi = \frac{I_{rms}^2}{I_{dc}^2} = \frac{\pi^4}{16m^2 \cos^2 \varphi} \cong \frac{6}{m^2 \cos^2 \varphi} \tag{22}$$

The factor ξ represents the increase of the MMC cells losses in comparison with a traditional VSI. As it can be noted, it is inversely proportional to m^2 and $\cos^2 \varphi$, assuming higher value at lower load power; at the maximum load power ($m = 1$ and $\cos \varphi = 1$) its value is around 6.

3.2.2. Sinusoidal Reference Voltage

For a sinusoidal shaped reference voltage, t_{on} can be calculated as:

$$v_{ref} = zV_{cell} + mzV_{cell} \cdot \sin(\omega t_{on}) = k \cdot V_{cell} \Rightarrow \omega t_{on} = \sin^{-1} \left(\frac{k - z}{mz} \right) \tag{23}$$

so that the DC current value of the generic k^{th} cell is:

$$I_{dc,k} = \frac{I_{pk}}{\pi} \cos \left[\sin^{-1} \left(\frac{k-z}{mz} \right) \right] \cos \varphi \quad z(1-m) < k \leq z(1+m) \quad (24)$$

Again, the cells DC current values distribution is elliptical with vertical and horizontal axes respectively equal to $I_{pk} \cdot \cos \varphi / \pi$ and mz . Thus, the quantity I_{dc} is:

$$I_{dc} = \frac{1}{N} \frac{1}{2} \cdot mz I_{pk} \cos \varphi = \frac{1}{4} m I_{pk} \cos \varphi \quad (25)$$

and, consequently, the ratio ξ becomes:

$$\xi = \frac{I_{rms}^2}{I_{dc}^2} = \frac{4}{m^2 \cos^2 \varphi} \quad (26)$$

The considerations regarding the triangular reference voltage case can be also applied to this case, with the difference that $\xi = 4$ (instead of about 6) at the maximum load power.

CONCLUSION

With reference to a Modular Multilevel Converter (MMC), this paper analyzed the current waveform of the current supplied by the electrochemical cells, both for triangular and sinusoidal reference voltage. Each cell current has been characterized by a different DC value and a different RMS value, and their distribution have been calculated. Moreover, a total DC current value has been derived expressing the total active power supplied by all cells and, analogously, a total RMS current value has been derived linked to the total cells losses.

Differently than in a traditional Voltage Source Inverter (VSI), in the case of MMC, the total RMS current value has been found not dependent on the modulation index or the power factor, determining augmented cell losses for the MMC in comparison with the VSI ones. In particular, for a given value of the load current peak value, the MMC cells losses depend only on the common mode component of the reference voltages, which is constrained if the converter DC-link is not isolated. Instead, in the case of an isolated DC-link, the reference voltage common mode component becomes a degree of freedom which could be exploited in order to minimize the cells losses.

CONSENT FOR PUBLICATION

Not applicable.

CONFLICT OF INTEREST

The authors declare no conflict of interest, financial or otherwise.

ACKNOWLEDGEMENTS

Propulsori elettrici ad eliche controrotanti per imbarcazioni e velivoli leggeri" financed by the Department of Electrical Engineering and IT of the University of Naples Federico II.

REFERENCES

- [1] Explaining road transport emissions, European Environment Agency - ISBN: 978-92-9213-723-6 - ORDER ID (Catalogue Number): TH-04-16-016-EN-N
- [2] J. Yun, T. Yeo, and J. Park, "High efficiency active cell balancing circuit with soft switching technique for series-connected battery string", *Power Electron. Conf. Expo.*, pp. 3301-3004 Long Beach, CA, USA
- [3] J. Kim, Shin C. Chun, and B.H. Cho, "Stable configuration of a Li-ion series battery pack based on a screening process for improved voltage/SOC balancing", *IEEE Trans. Power Electron.*, vol. 27, no. 1, pp. 411-424, 2012. [<http://dx.doi.org/10.1109/TPEL.2011.2158553>]

- [4] M. Daowd, M. Antoine, N. Omar, P. Van Den Bossche, and J. Van Mierlo, "Single switched capacitor battery balancing system enhancements", *Energies*, vol. 6, no. 4, pp. 2149-2174, 2013. [<http://dx.doi.org/10.3390/en6042149>]
- [5] H. Rahimi-Eichi, U. Ojha, F. Baronti, and M.Y. Chow, "Battery Management System: An Overview of Its Application in the Smart Grid and Electric Vehicles", *IEEE Ind. Electron. Mag.*, vol. 7, no. 2, pp. 4-16, 2013. [<http://dx.doi.org/10.1109/MIE.2013.2250351>]
- [6] A. Emadi, K. Rajashekar, S.S. Williamson, and S.M. Lukic, "Topological overview of hybrid electric and fuel cell vehicular power system architectures and configurations", *IEEE Trans. Vehicular Technol.*, vol. 54, no. 3, pp. 763-770, 2005. [<http://dx.doi.org/10.1109/TVT.2005.847445>]
- [7] G. Brando, A. Dannier, A. Del Pizzo, R. Rizzo, and I. Spina, "Torque derivative control in induction motor drives supplied by multilevel inverters", *IET Power Electron.*, vol. 9, no. 11, pp. 2249-2261, 2016. [<http://dx.doi.org/10.1049/iet-pel.2014.0958>]
- [8] G. Brando, A. Dannier, A. Del Pizzo, R. Rizzo, and I. Spina, "Generalised look-up table concept for direct torque control in induction drives with multilevel inverters", *IET Electr. Power Appl.*, vol. 9, no. 8, pp. 556-567, 2015. [<http://dx.doi.org/10.1049/iet-epa.2014.0488>]
- [9] L.M. Tolbert, Z.P. Fang, and T.G. Habetler, "Multilevel converters for large electric drives", *IEEE Trans. Ind. Appl.*, vol. 35, no. 1, pp. 36-44, 1999. [<http://dx.doi.org/10.1109/28.740843>]
- [10] L.M. Tolbert, J.N. Chiasson, K.J. McKenzie, and Z. Du, "Control of cascaded multilevel converters with unequal voltage sources for HEVs", *Electric Machines and Drives Conference*, vol. 2, pp. 663-669, 2003.
- [11] G. Brando, A. Dannier, Spina I, and Tricoli P, "Integrated BMS-MMC balancing technique highlighted by a novel space-vector based approach for BEVs application", *Energies*, vol. 10, no. 10, p. 1628, 2017. [<http://dx.doi.org/10.3390/en10101628>]
- [12] X. Liu, A. Lindemann, and H. Amiri, "Theoretical and experimental comparison of different control strategies for modular multilevel converters", In: *Proc. IEEE 15th Workshop Control Model. Power Electron.*, Jun. 22-25, 2014, pp. 1-9.
- [13] M. Quraan, T. Yeo, and P. Tricoli, "Design and control of modular multilevel converters for battery electric vehicles", *IEEE Trans. Power Electron.*, vol. 31, no. 1, pp. 507-515, 2016. [<http://dx.doi.org/10.1109/TPEL.2015.2408435>]
- [14] M. Tsirinomeny, and A. Rufer, "Configurable Modular Multilevel Converter (CMMC) for flexible EV", In: *2015 17th European Conference on Power Electronics and Applications (EPE'15 ECCE-Europe)*, Geneva, 2015. [<http://dx.doi.org/10.1109/EPE.2015.7309229>]
- [15] M. Quraan, P. Tricoli, S. D'Arco, and L. Piegari, "Efficiency Assessment of Modular Multilevel Converters for Battery Electric Vehicles", *IEEE Trans. Power Electron.*, vol. 32, no. 3, pp. 2041-2051, 2017. [<http://dx.doi.org/10.1109/TPEL.2016.2557579>]
- [16] S. D'Arco, L. Piegari, and P. Tricoli, "A modular converter with embedded battery cell balancing for electric vehicles," *2012 Electrical Systems for Aircraft*, Railway and Ship Propulsion: Bologna, 2012, pp. 1-6.
- [17] F. Ciccarelli, A. Del Pizzo, and D. Iannuzzi, "An ultra-fast charging architecture based on modular multilevel converters integrated with energy storage buffers", *2013 Eighth International Conference and Exhibition on Ecological Vehicles and Renewable Energies (EVER)*, 2013pp. 1-6 Monte Carlo